




Investigating the Relationship between Urbanization and Air Pollution Using Google Earth Engine Platform: A Case Study of Istanbul

Duygu Yasan¹, Uğur Acar^{2,*}, Osman Salih Yılmaz³

¹ Survey-Land Registry - Cadastre, Bahcecik Vocational and Technical Anatolian High School, Kocaeli, Türkiye

² Geomatic Engineering Department, Faculty of Civil Engineering, Yildiz Technical University, Istanbul, Türkiye

³ Department of Geographic Information System, Demirci Vocational School, Manisa Celal Bayar University, Manisa, Türkiye

* Corresponding author: U. Acar
E-mail: uacar@yildiz.edu.tr

Received 08.08.2023
Accepted 15.09.2024

How to cite: Yasan et al., (2024). Investigating the Relationship between Urbanization and Air Pollution Using Google Earth Engine Platform: A Case Study of Istanbul, *International Journal of Environment and Geoinformatics (IJEGEO)*, 11(3): 130-146. doi. 10.30897/ijegeo.1339560

Abstract

Rapid population growth, industrialization, urbanization, loss of green areas, increased vehicle traffic, and heightened fossil fuel consumption in megacities like Istanbul have led to various impacts. These effects contribute to an increase in air pollution within urban areas. Rapid urbanization and heightened air pollution in megacities can lead to serious environmental, economic, and health problems. Therefore, understanding this relationship and identify its impacts is crucial. This study aims to examine the relationship between urbanization and air pollution in Istanbul. For this purpose, land cover maps covering Istanbul province were produced using Landsat-5 (TM), Landsat-8 (OLI), and Sentinel-2 (MSI) images from the years 1996 to 2021, at three-year intervals, on the Google Earth Engine platform. Land cover for classification purposes was divided into five different classes: forest, water surface, urban area, bare land, and classified using a random forest machine learning algorithm. To examine the impact of urban area growth on air pollution, the second step of the study involved analyzing the column number density values of SO₂, NO₂, CO, and O₃ gases from Sentinel-5P (TROPOMI) data for the years 2019, 2020, and 2021. The averages of the data from 39 air pollution monitoring stations across Istanbul were also examined. According to this classification, the urban area expanded from 491 km² in 1996 to 1222 km² by 2021. Considering the total surface area of Istanbul province, the proportion of urban area increased from 9% in 1996 to 23% by 2021. The TROPOMI values were calculated as follows: the average column number density values for SO₂, NO₂, CO, and O₃ were 0.0003538 mol/m², 0.0339514 mol/m², 0.0000984 mol/m², and 0.1453515 mol/m², respectively. Similarly, the gas concentrations of SO₂, NO₂, CO, and O₃ measured from the ground stations were calculated as 6.603 μ/m³, 786,815 μ/m³, 43.763 μ/m³ and 45.773 μ/m³, respectively. Correlations between urbanization and TROPOMI values revealed a positive correlation of 0.39, 0.02, and 0.80 for SO₂, NO₂, and CO gases, while a negative correlation of 0.25 was found for O₃ gas. The study also examined correlations between TROPOMI and ground station measurements, resulting in positive correlations of 0.55, 0.66, and 0.16 for SO₂, NO₂, and CO gases, respectively, while a negative correlation of 0.05 was found for O₃ gas. Based on these findings, among the air pollutants studied both through TROPOMI and ground station data, the highest correlation was observed for CO gas. These results provide an important source of information for understanding the environmental impacts of the urbanization process in megacities and for developing strategies to reduce air pollution. They also demonstrate that methods such as remote sensing and atmospheric data analysis are effective tools for understanding and solving environmental problems.

Keywords: Istanbul, TROPOMI, Sentinel 5P, Google Earth Engine, Air pollution, Random Forest

Introduction

Urban areas have the most dynamic structures in the world, and their dimensions continuously increase in parallel with global population growth. Owing to the lack of a standard policies and guidelines for building construction and urban planning, cities tend to experience irregular growth (Duran and Özkan, 2015). In these regions, problems such as excessive concreting, intense industrialization, and heavy traffic have led to air pollution (Wang and Hao, 2012). Rapidly growing cities worldwide have become a major concern and require close monitoring. Urbanization driven by population growth, especially in large cities, leads to significant pollution issues (Grimm et al., 2008; Kural et al., 2018; Ülker et al., 2021). The decrease in air quality leads to the deterioration of ecological balance and poses a threat to human health (Tyagi et al., 2014). In January 2021, a

report on Air Pollution and COVID-19 by the European Parliament's Committee on Environment, Public Health, and Food Safety highlighted that fine particulate matter (PM) pollution alone causes approximately 400,000 premature deaths annually in Europe and over 4,000,000 worldwide. Prolonged exposure to air pollution, including fine PM_{2.5}, with a diameter smaller than 2.5 μm and ozone (O₃), is estimated to result in 8.8 million excess deaths annually, while nitrogen dioxide (NO₂) contributes to four million new pediatric asthma cases per year (Achakulwisut et al., 2019; Burnett et al., 2018; Lelieveld et al., 2020). Considering these findings, the management and control of air quality has become increasingly critical globally, affecting both citizens and policymakers. Therefore, monitoring urban changes and air quality using remote sensing (RS) techniques has become increasingly practical (Raja et al., 2013). RS technology provides powerful tools for monitoring environmental and land

use/cover changes (Alqurashi and Kumar, 2013). The information obtained from RS data plays a crucial role in measuring and understanding the nature and location of changes in land cover (Yuan et al., 2005). Such information is essential for planning urban growth and development (Yuan et al., 2005). Advancements in satellite technology have made it easier to acquire and analyze data related to urbanization and its. Land use maps can be created using images acquired from satellites and classification methods (Saadat et al. 2011).

Air quality has traditionally been monitored through ground-based monitoring station networks. However,, there are numerous studies focused on using RS technologies (Engel-Cox et al., 2004; Gupta et al., 2006; Martin, 2008; Tømmervik et al., 1995). Several satellite sensor systems, such as SCanning Imaging Absorption spectroMeter for Atmospheric CHartographY (SCIAMACHY), the Global Ozone Monitoring Experiment (GOME), Ozone Monitoring Instrument (OMI), and TROPOspheric Monitoring Instrument (TROPOMI), are used to monitor the concentration of air pollutants (Huang and Sun, 2020). TROPOMI has been providing data since mid-2018 and has a spatial resolution of 5.5 km × 3.5 km (Kang et al., 2021).

RS studies, especially for large-scale areas, require high-speed, large-storage-capacity computers to download, process, and analyze numerous satellite images. The Google Earth Engine (GEE), along with other vector data, facilitates the processing of petabytes of image data in a cloud environment (Guo et al., 2022; Yilmaz et al., 2023). The most prominent feature that distinguishes the GEE platform from other software is its elimination of the need to download the satellite images. As a result, storage requirements, computer hardware, and software needs are significantly reduced. Additionally, it saves user time by removing the need for repeated analysis (Kumar and Mutanga, 2018; Gorelicck et al., 2017).

The GEE platform has been utilized in numerous studies, including mapping agricultural lands (Dong et al., 2016), monitoring changes in urban land-use areas (Patel et al., 2015), extracting coastal zones (Vos et al., 2019), conducting flood prevention and emergency response studies (Vos et al., 2019), and detecting oil platforms (Wong et al., 2019). Numerous studies have been conducted on the GEE platform at both regional and global scales, focusing on topics such as the identification of urban land-use areas and urban growth. Patel et al. (2015) classified urban land use areas on Java Island, Indonesia, using the Normalized Difference Spectral Vector (NDSV) method and Landsat 5 and 7 data from the GEE catalog. The study underwent statistical evaluation, and the effectiveness of population mapping methods was examined to validate these urban extents. The results of the study concluded that automatic classification using GEE produced accurate urban land cover maps, and that integrating urban extents derived from GEE improved the quality of population mapping. Aghlmand et al. (2021) produced land use maps using the GEE platform. For this purpose, they utilized all images acquired by the Landsat-8, Sentinel-1, and Sentinel-2

satellites between 2019 and 2020. In this study, five different indices, namely the normalized difference vegetation index (NDVI), enhanced vegetation index (EVI), normalized difference water index (NDWI), normalized difference built-up index (NDBI), and urban index (UI), were employed along with the support vector machine (SVM) algorithm for 19 different combinations. Five distinct land classes were identified: urban areas, roads, water bodies, forests, agricultural lands, and bare lands. The best classification performance was achieved with a combination of NDVI from Landsat-8 and NDVI, NDBI, UI, and NDWI from Sentinel-2 and Sentinel-1 (VV). In this combination, the overall accuracy was 96.62, and the kappa coefficient was 95.76. Liu et al. (2020) conducted large-scale urban land mapping of China's Middle Yangtze River basin, covering an area of 317,000 km². They used OpenStreetMap (OSM) data integrated with Landsat images on the GEE platform for the period between 1987 and 2017. Training samples for the most recent year were generated based on updated OSM land use data after a manual topological alignment process, and then uploaded to GEE for automatic image classification. When compared with the independent samples, the overall accuracies and kappa coefficients for all years ranged from 98% to 99% and 0.65 to 0.85, respectively. Liu et al. (2018), using the GEE platform, produced global urban land use maps for the period between 1990 and 2010, with five-year intervals, utilizing Landsat images and the normalized urban areas composite index (NUACI) method. The overall accuracy (OA), producer's accuracy (PA), and user's accuracy (UA) of the study were found to 0.81-0.84, 0.5-0.60, and 0.49-0.61, respectively. The analysis revealed that the global urban land area increased from 450.97±1.18 thousand km² in 1990 to 747.05±1.50 thousand km² in 2010, covering 0.63% of the global land areas. Additionally, various studies have utilized data from Sentinel-5P TROPOMI for air pollution monitoring. Kaplan and Avdan (2020) investigated the average atmospheric NO₂ and CO concentration values obtained by Sentinel-5P TROPOMI over the Republic of North Macedonia for a period of six months. They examined the relationship between these data, and geographic and demographic factors. The analysis revealed a strong positive correlation (R = 0.78) between NO₂ concentrations and population statistics, and a strong negative correlation (R = -0.9) between altitude and CO values. Potts et al. (2021) conducted a study in satellite observations of tropospheric NO₂ were obtained from TROPOMI and the Goddard Earth Observing System (GEOS)-Chem 3D chemical transport model. The study revealed a 20% decrease in NO₂ concentrations across the country during the lockdown period (March 23-May 31, 2020). Magro et al. (2021) monitored CO and CH₄ concentrations after a fire incident in Portugal using Sentinel-5P satellite images and evaluated the performance of TROPOMI. They investigated the spatial distributions of CO and CH₄ before, during, and after a fire event. On July 21, 2019, and August 7, 2019, CO concentrations exceeding 4.5x10¹⁸ and 6x10¹⁸ mol/cm² were observed, respectively. Sünsüli and Kalkan (2022) conducted a comparative analysis of tropospheric NO₂ levels in the Marmara Region before and during the COVID-19 pandemic (late 2019, 2020, and 2021) using

Sentinel-5P satellite imagery. They identified the adverse effects of fossil fuel consumption on air quality, and the satellite data demonstrated a high correlation ($r=0.85$) with data obtained from ground measurement stations. As a result, Sentinel-5P satellite imagery was shown to be an effective tool for monitoring air pollution. Yilmaz et al. (2023) investigated the emission of pollutant gases following forest fires in the Mediterranean using Sentinel-5P TROPOMI instrument in the year 2021. They observed that pre-fires, the tropospheric CO column number density in all burned areas was 0.03 mol/m^2 , whereas post-fires, this value increased to 0.14 mol/m^2 . Furthermore, by analyzing Sentinel-5P data over a larger area, they observed that the amount of CO increased up to a maximum value of 0.333 mol/m^2 . Cakmak et al. (2023) investigated variations in NO_2 , CO, and SO_2 pollutant gases between June 2019 and June 2021 during the COVID-19 pandemic. Using the GEE platform, they calculated the average column density values of NO_2 , CO and SO_2 in the Marmara Region for the selected dates as $8.40\text{E-}05 \text{ mol/m}^2$, $3.23\text{E-}02 \text{ mol/m}^2$ and $3.75\text{E-}04 \text{ mol/m}^2$, respectively. During the quarantine period, these values decreased to $7.84\text{E-}05 \text{ mol/m}^2$, $3.05\text{E-}02 \text{ mol/m}^2$ and $2.75\text{E-}04 \text{ mol/m}^2$, respectively.

The temporal changes in urban growth in Istanbul Province were analyzed using Landsat-5 (TM), Landsat-8 (OLI), and Sentinel-2 (MSI) imagery through a supervised classification method on the GEE platform. Land use maps from 1996 to 2021 were generated in GEE using JavaScript (JS) code. The study examined the relationship between urban growth data derived from the classification and the levels of SO_2 , CO, NO_2 , and O_3 obtained from TROPOMI Sentinel-5P and ground-based monitoring stations. Additionally, the relationship between TROPOMI data and urban growth was analyzed for the period 2019–2021, while gas concentration data was analyzed for the period 2013–2021. As a result of these analyses, the relationship between air pollutants and urbanization was evaluated on a monthly, annual, and seasonal basis. Unlike previous studies, this research is innovative in its examination of the relationship between urban growth and pollutant gases.

Materials and Methods

Istanbul is the most populous province in Türkiye and receives the highest migration, with most of its economy based on industry and trade. According to the 2021 Address-Based Population Registration System (ABPRS) prepared by the Turkish Statistical Institute (TURKSTAT), the total population of Istanbul is 15,840,900 (URL-1). The city covers an area of 5,461 km^2 and is in the northwestern part of Türkiye, spanning both the European and Asian continents. Istanbul has a temperate climate, exhibiting transitional characteristics between the Black Sea climate and the Mediterranean climate. The temperature ranges from an average of 2°C to 28°C (URL-2), and the total annual precipitation is 843.9 mm, occurring throughout the year (URL-3; Arslan and Akyürek, 2018).

In this study, classification and gas concentration maps were created for Istanbul Province. The study area includes the administrative borders of Istanbul Province. In the spatial analyses, the same boundaries were used for all factors. Figure 1 shows a map of the provincial border of Istanbul in the study area.

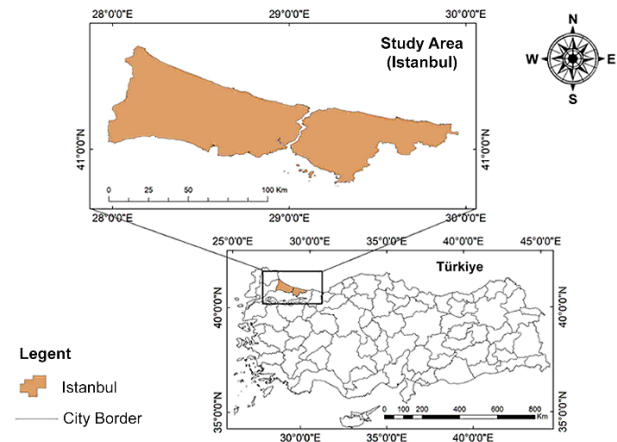


Fig. 1. Study area

In this study, Landsat-5 (TM), Landsat-8 (OLI) and Sentinel-2 (MSI) images provided by the joint program of the National Aeronautics and Space Administration (NASA) and the United States Geological Survey (USGS) were used to produce land use maps. Details about the corrected images obtained from the GEE platform are shown in Table 1.

Table 1. Satellite images used

Collection name	GEE Image Collection ID	Data Availability
Landsat-5 (TM)	LANDSAT/LT05/C01/T1_TOA	January 1, 1984 - May 5, 2012
Landsat- 8 (OLI)	LANDSAT/LC08/C01/T1_TOA	April 11, 2013-
Sentinel- 2 (MSI)	COPERNICUS/S2	June 23, 2015-
Sentinel- 2 (MSI)	COPERNICUS/S2_SR	March 28, 2017-

In the Türkiye, air pollution is measured and monitored by the Ministry of Environment, Urbanization, and Climate Change. The National Air Quality Index (NAQI) was developed based on the air quality index used by the United States Environmental Protection Agency (US EPA) and tailored to national regulations and limit values. The air quality index is calculated for five primary pollutants: Particulate Matter (PM), CO, SO_2 , NO_2 , and O_3 . NAQI values provide general information about the air quality of a specific region, issue warnings in the case of poor air quality, and recommend the necessary measures.

In this study, land use maps based on Landsat-5 (TM), Landsat-8 (OLI), and Sentinel-2 images were generated using JS code on the GEE platform for the period 1996-2021 in Istanbul province at three-year intervals. Three different indices were calculated in the study: NDVI,

NDWI, and NDBI. These indices, along with the visible (VIS) and near-infrared (NIR) bands, were used to classify Istanbul into five different land-use categories: forest, water bodies, urban areas, bare land, and agricultural land. Homogenously distributed samples were collected in the study area and classified using the Random Forest (RF) machine learning algorithm. The RF algorithm is an ensemble learning technique based on bagging integration. The RF algorithm is often used in regression analysis and in land-cover classification studies. The RF algorithm is often preferred for the processing of large volumes of remote-sensing satellite data in terms of simple parameter settings, noise reduction, and low computing costs (He et al., 2019). On average, 100 training data points and 80 test data points were used for each year. Finally, the producer's accuracy (PA), user's accuracy (UA), overall accuracy (OA), and Kappa (K) statistics were calculated for the classification results. The classification workflow is illustrated in Figure 2.

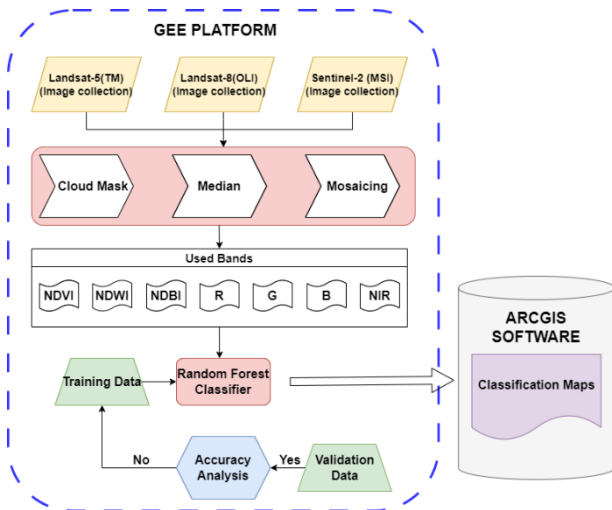


Fig. 2. Classification workflow chart

To investigate the relationship between urbanization and air pollution, monthly column number density values for SO₂, NO₂, CO and O₃ gases for the years 2019, 2020, and 2021 were first obtained from GEE platform. Additionally, gas concentration values were collected from air monitoring stations in Istanbul to further explore this relationship. The workflow for obtaining and analyzing these values is shown in Figure 3.

Results

Land classification maps were generated on the GEE platform using JS and satellite images for the years 1996, 2003, 2007, 2011, 2013, 2015, 2016, 2017, 2018, 2019, 2020, and 2021. In the study, maps belonging to five different land classes were created: forest, water surface, urban area, agricultural land, and bare land. The accuracy analysis of the classification was performed for each year. The PA values in the classes vary between 83.73% and 100%, while the UA values vary between 78.92% and 100%. The OA value was over 90%. According to these results, it can be said that the classification made was

successful. The accuracy assessment of the classification for all years is given in Table 2.

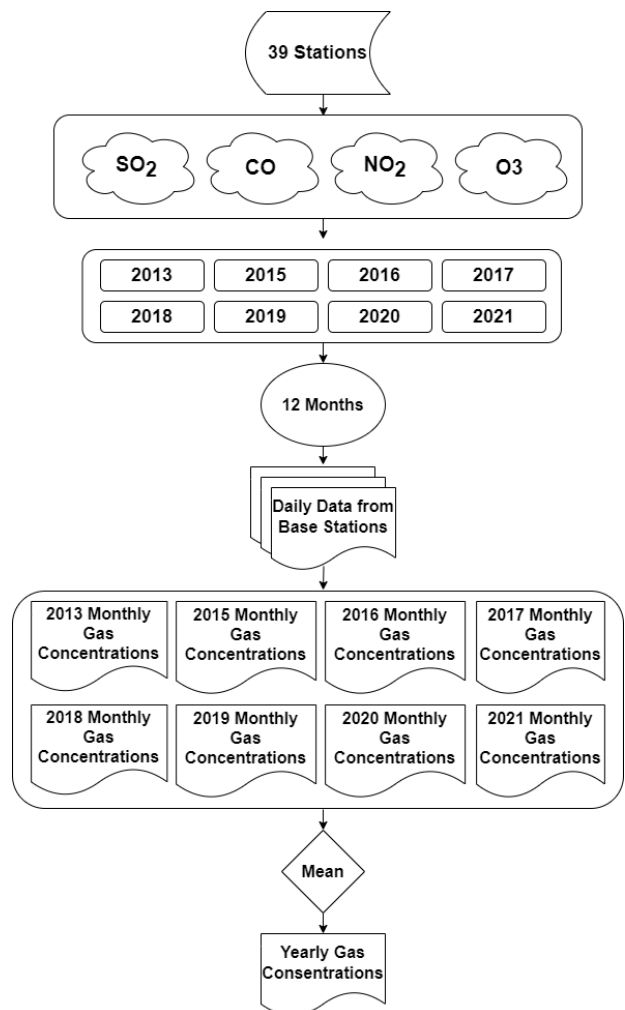


Fig. 3. Ground stations gas concentration workflow

Upon examining the classification results, it is observed that forest and water areas show relatively little variation, while bare land and agricultural areas have decreased over time. On the other hand, urban areas exhibit a notable increase, progressing mostly from the southern to the northern regions of the city. The distinctive expansion of red-colored urban areas from 1996 to 2021 is evident. Additionally, an increase in urban areas is accompanied by a decrease in yellow-colored vacant areas and green-colored agricultural lands. Detailed land classification area change values are presented in Table 3. Furthermore, annual land class change graphs are shown in Figure 4, and the corresponding maps are displayed in Figure 5.

Monthly column number density values for the years 2019, 2020, and 2021 were obtained on the GEE platform. The 3-year average column number density for each month was calculated by averaging the monthly values across the three years, based on TROPOMI data (Table 4).

The monthly gas column number density changes graphs based on TROPOMI for the 3-year period, using the gas column number density values from Table 4, are presented in Figure 6.

Table 2. Accuracy assessment of classification

Date	Classes	PA (%)	UA (%)	OA (%)	K
1996	Forest	99.57	98.93	92.93	0.94
	Water	100.00	100.00		
	Urban	84.59	91.77		
	Agriculture	83.73	78.92		
	Bare land	97.93	95.07		
2003	Forest	99.14	81.96	91.17	0.87
	Water	99.77	99.68		
	Urban	86.39	95.44		
	Agriculture	85.32	59.33		
	Bare land	92.41	95.86		
2007	Forest	99.90	98.08	91.27	0.87
	Water	97.43	98.54		
	Urban	85.19	94.66		
	Agriculture	78.79	63.55		
	Bare land	94.48	93.68		
2011	Forest	100.00	89.56	92.72	0.91
	Water	99.59	100.00		
	Urban	89.19	85.34		
	Agriculture	80.69	84.89		
	Bare land	88.66	94.93		
2013	Forest	99.72	99.17	92.06	0.90
	Water	99.51	99.64		
	Urban	83.03	93.67		
	Agriculture	86.59	81.97		
	Bare land	93.09	82.59		
2015	Forest	99.96	93.11	93.39	0.90
	Water	99.84	99.43		
	Urban	87.01	89.61		
	Agriculture	80.46	86.91		
	Bare land	93.66	95.33		
2016	Forest	99.80	98.98	95.81	0.93
	Water	96.85	100.00		
	Urban	95.04	80.83		
	Agriculture	78.17	85.65		
	Bare land	90.65	97.24		
2017	Forest	100.00	97.00	96.12	0.94
	Water	100.00	100.00		
	Urban	91.26	83.40		
	Agriculture	87.77	98.60		
	Bare land	92.20	96.37		
2018	Forest	99.65	90.88	91.99	0.89
	Water	100.00	100.00		
	Urban	91.10	70.94		
	Agriculture	78.20	88.82		
	Bare land	91.78	98.27		
2019	Forest	90.82	81.77	90.41	0.86
	Water	95.71	99.12		
	Urban	94.26	84.05		
	Agriculture	66.09	88.74		
	Bare land	91.54	93.91		
2020	Forest	99.61	82.32	90.47	0.87
	Water	99.88	99.99		
	Urban	96.06	79.69		
	Agriculture	66.95	92.25		
	Bare land	87.35	96.92		
2021	Forest	98.15	86.27	91.10	0.87
	Water	99.91	99.99		
	Urban	96.98	81.14		
	Agriculture	60.25	84.72		
	Bare land	88.89	96.70		

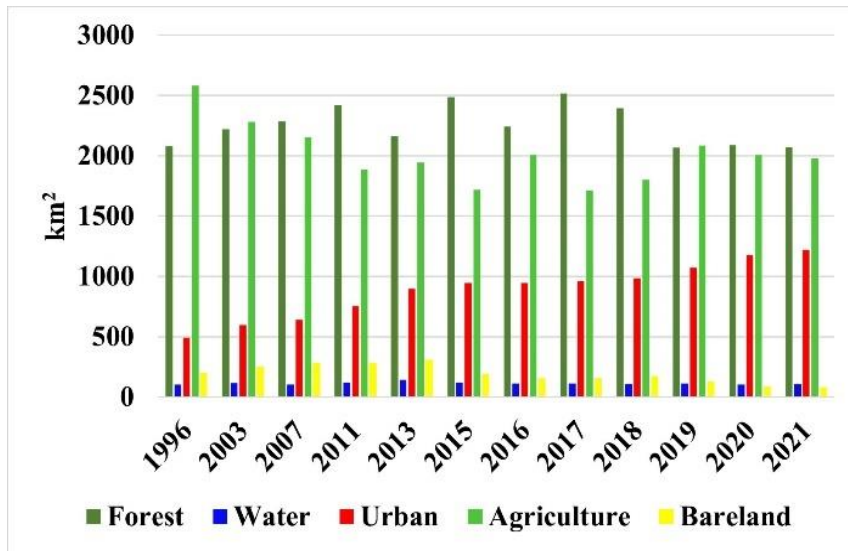


Fig. 4. Classification area change graph

Table 3. Areas obtained as a result of classification

Date	Forest (km ²)	Water (km ²)	Urban (km ²)	Agriculture (km ²)	Bare land (km ²)
1996	2081	105	491	2581	201
2003	2218	115	594	2281	251
2007	2283	101	641	2153	281
2011	2419	120	751	1886	283
2013	2163	144	897	1945	310
2015	2485	121	943	1719	191
2016	2240	111	946	2006	156
2017	2517	112	964	1711	155
2018	2395	107	985	1800	172
2019	2067	110	1071	2082	129
2020	2087	103	1176	2006	87
2021	2072	107	1222	1978	80

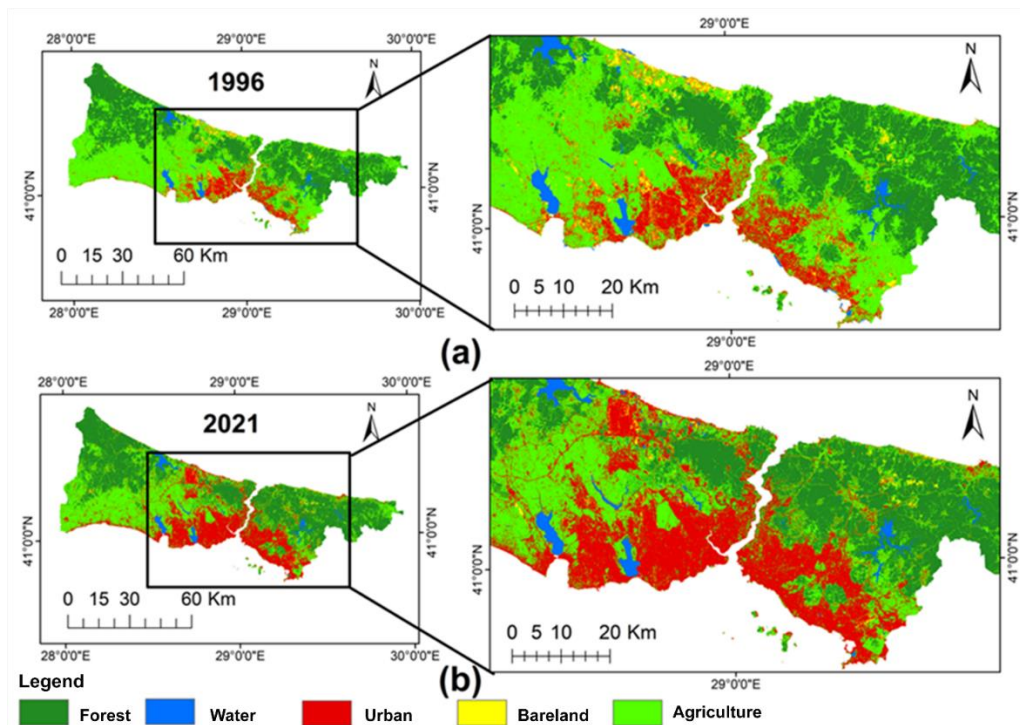


Fig. 5. Satellite image classification maps classified using the RF algorithm: a) classification map dated 1996 (Landsat-5) b) classification map dated 2021 (Sentinel-2)

Table Hata! Belgede belirtilen stilde metne rastlanmadı.. 3-year (2019-2020-2021) average column number density based on TROPOMI

Months	SO ₂ (mol/m ²)	NO ₂ (mol/m ²)	CO (mol/m ²)	O ₃ (mol/m ²)
January	1.057E-03	1.047E-04	3.496E-02	1.550E-01
February	6.797E-04	1.163E-04	3.616E-02	1.540E-01
March	4.284E-04	1.066E-04	3.748E-02	1.607E-01
April	1.968E-04	1.006E-04	3.855E-02	1.628E-01
May	2.002E-04	9.645E-05	3.431E-02	1.521E-01
June	1.134E-04	9.674E-05	3.123E-02	1.495E-01
July	1.524E-04	8.821E-05	3.090E-02	1.399E-01
August	8.590E-05	8.778E-05	3.312E-02	1.356E-01
September	1.062E-04	8.928E-05	3.302E-02	1.334E-01
October	3.053E-04	9.432E-05	3.185E-02	1.295E-01
November	6.170E-04	1.165E-04	3.180E-02	1.381E-01
December		1.177E-04	3.312E-02	1.417E-01

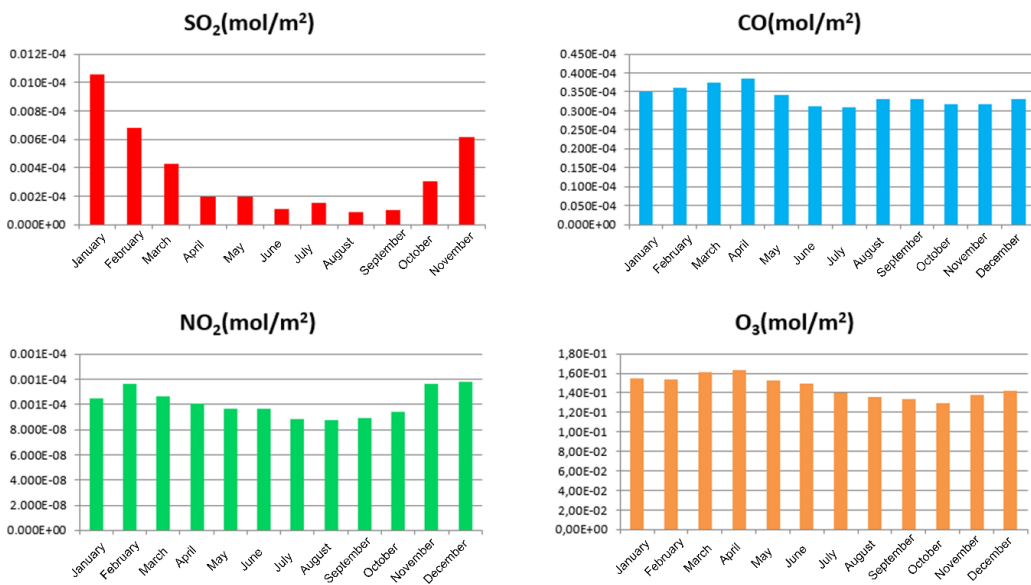


Fig. 6. The 3-year average monthly column number density for SO₂, NO₂, CO and O₃ based on TROPOMI data.

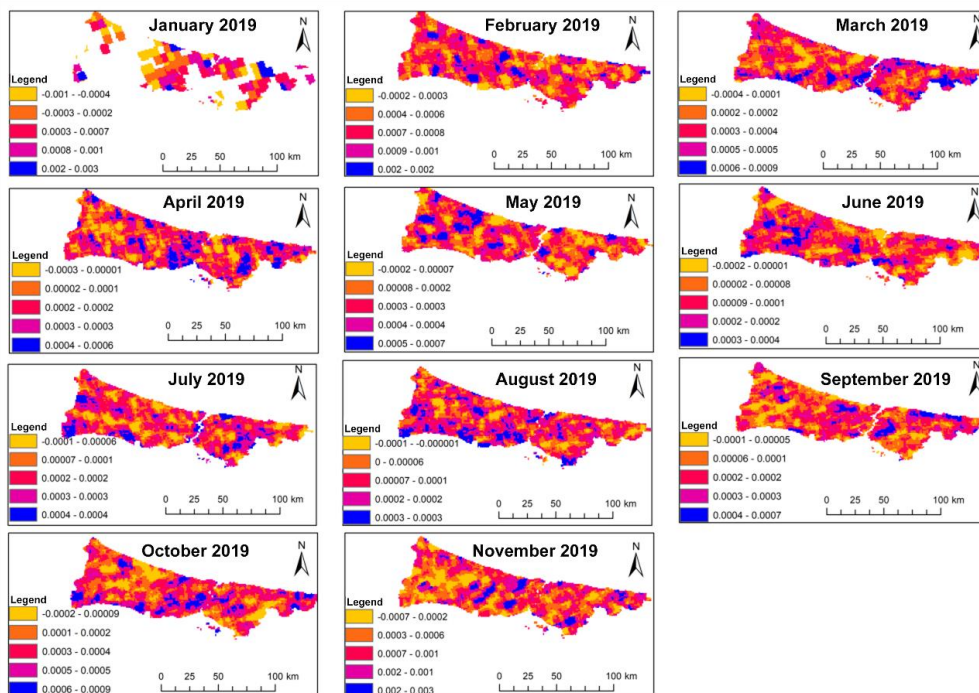


Fig. 7. TROPOMI SO₂ column number density map for 2019

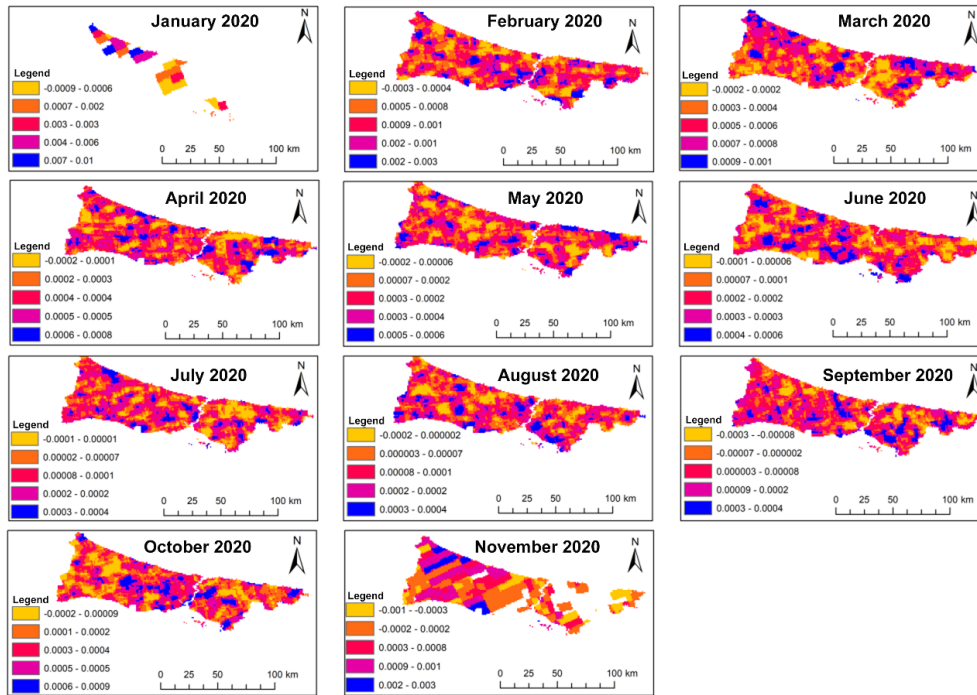


Fig. 8. TROPOMI SO₂ column number density map for 2020

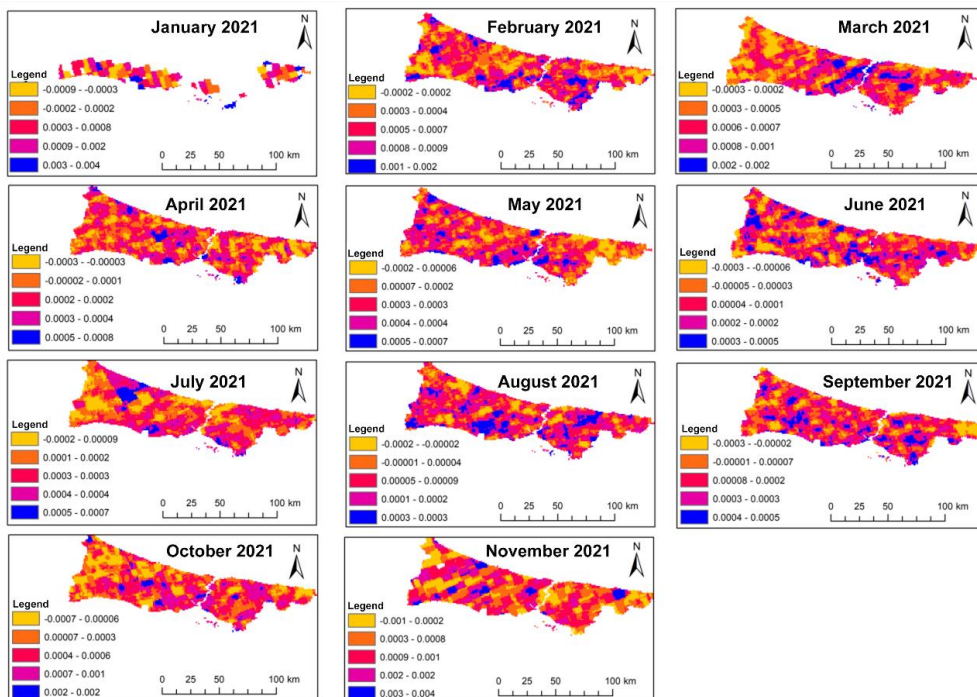


Fig. 9. TROPOMI SO₂ column number density map for 2021.

Monthly column number density changes maps for the years 2019, 2020, and 2021 were generated on the GEE platform using JS code (Figure 7, 8, and 9). When examining the TROPOMI-based Istanbul maps for SO₂ gas, it is observed that the gas has both its lowest and highest values in November and January. Considering the TROPOMI-based average values, SO₂ gas reaches low levels during the summer months and its highest levels during the winter months. However, within the city, a different distribution pattern was observed. In the month

with the highest SO₂ levels, the lowest values could be observed in another region of the city. Furthermore, it was found that the areas with high column number density value of SO₂ (indicated by the blue color) and the areas with low column number density (indicated by the yellow color) were overlapping, revealing significant variability in gas column number density within the city. This finding makes it challenging to provide a definitive interpretation about the specific regions of high and low SO₂ levels over Istanbul.

When the TROPOMI-based Istanbul maps for NO₂ gas are examined, it is observed that the gas has its lowest values in the summer months, such as June, July, and August, and its highest value in the winter month of February over a three-year period (Figure 10,11,12). According to the previous section, when considering the TROPOMI-based average values, NO₂ gas reaches its lowest levels in the summer months and its highest levels

in the winter months. This situation is also similar within the city. It has been determined that the column number density of NO₂ gas, unlike SO₂ gas, is sharply separated over the city. Based on this, it can be said that areas with high NO₂ (blue) are located in coastal regions where urbanization and, consequently, human activities are high, whereas areas with low NO₂ (yellow) are found in the eastern and western parts of the city where urbanization is low and agricultural lands are more prevalent.

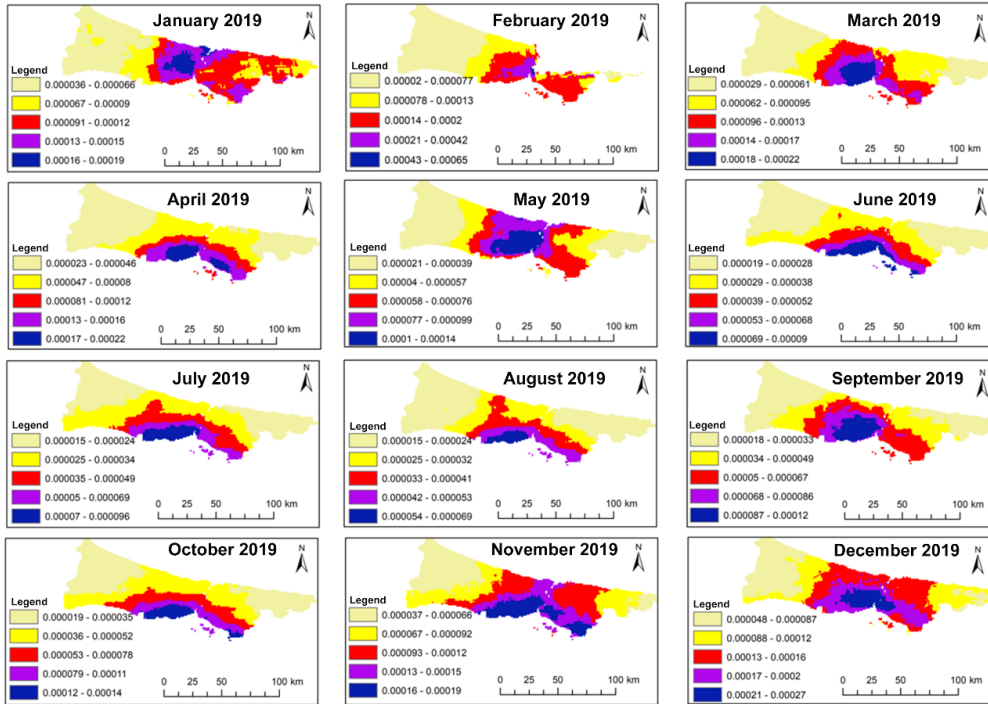


Fig. 10. TROPOMI NO₂ column number density map for 2019

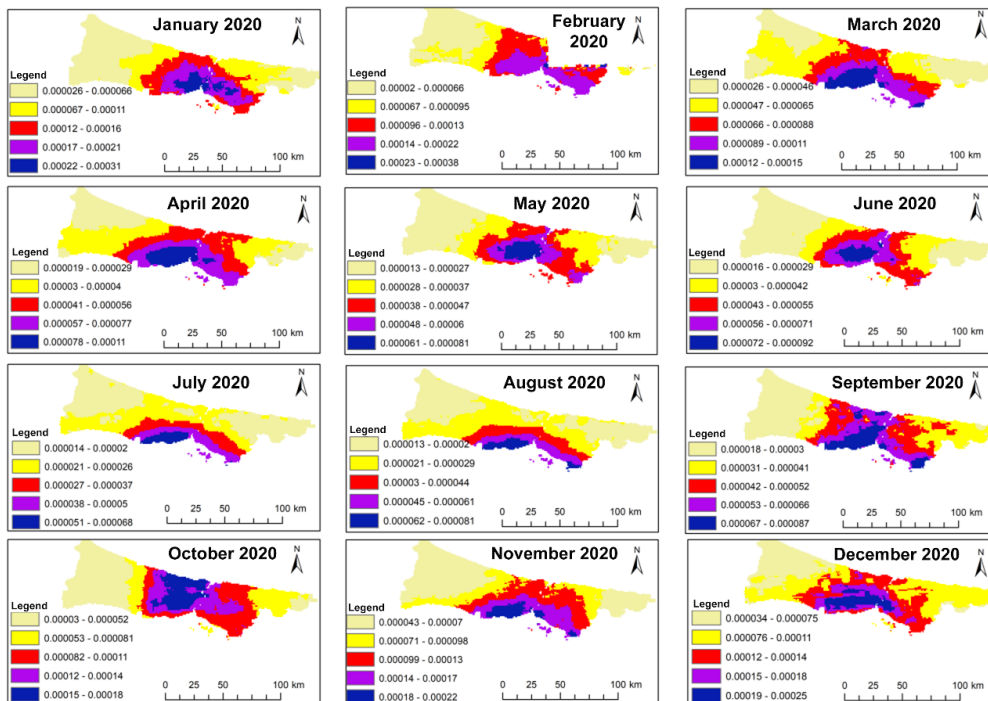


Fig. 11. TROPOMI NO₂ column number density map for 2020

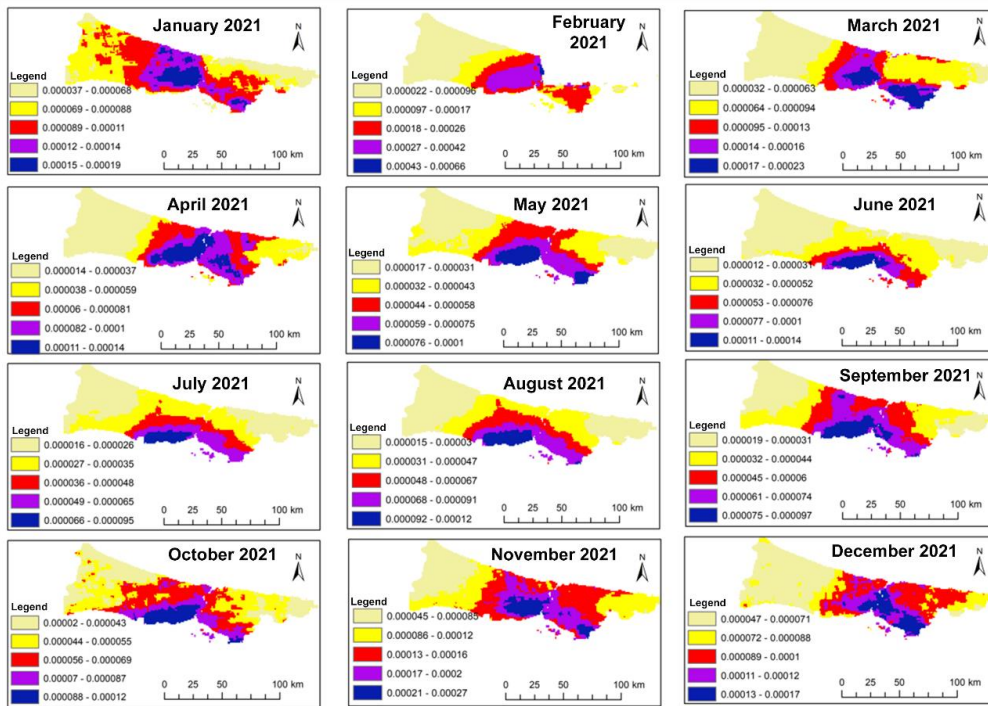


Fig. 12. TROPOMI NO₂ column number density map for 2021.

When the TROPOMI-based Istanbul maps for the CO gas are examined, it is observed that the gas has its lowest values mostly in July, while its highest value vary between March and April (Figure 13,14,15). According to the previous section, when considering the TROPOMI-based average values, CO gas reaches its lowest levels in the summer months and its highest levels in the spring months. This situation is also similar within the city. CO

gas shows a notable variation in column number density, although not as pronounced as for SO₂ gas. It has been determined that the areas with high column number density (orange) and the areas with low column number density (blue) are intermingled. This situation has not made it possible to make a clear comment on the regions where the CO gas is high and low in Istanbul.

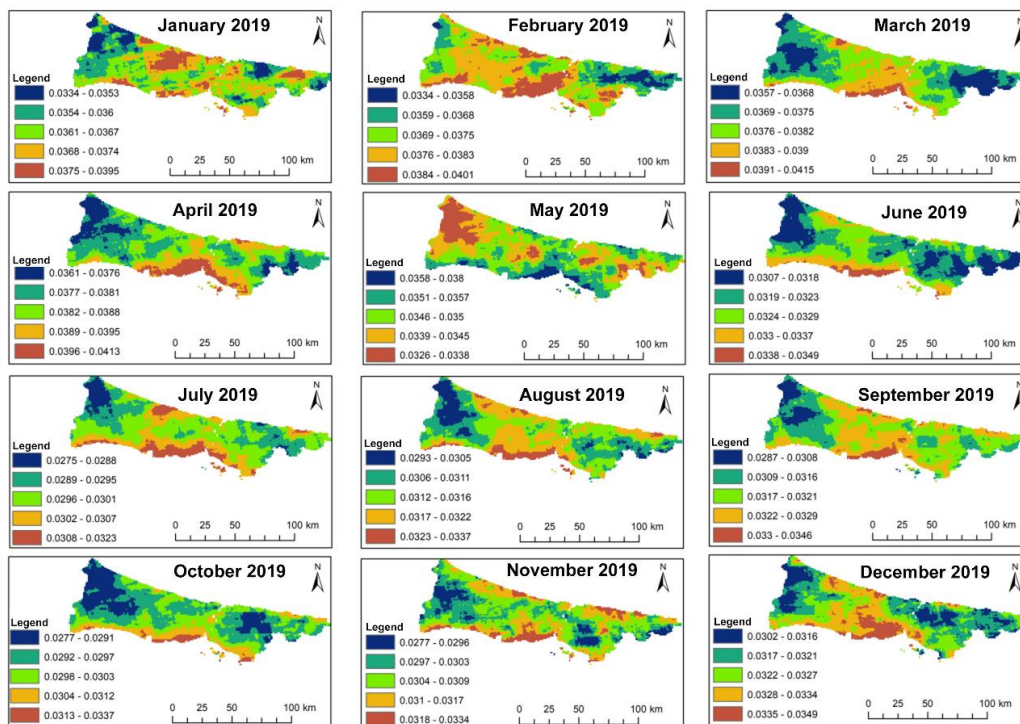


Fig. 13. TROPOMI CO column number density map for 2019

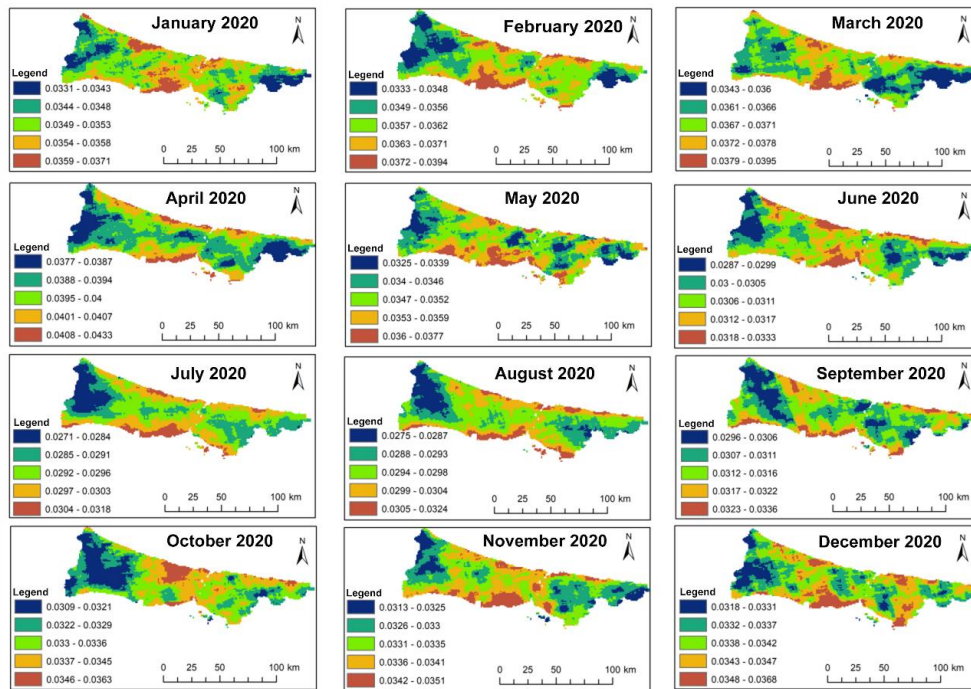


Fig. 14. TROPOMI CO column number density map for 2020

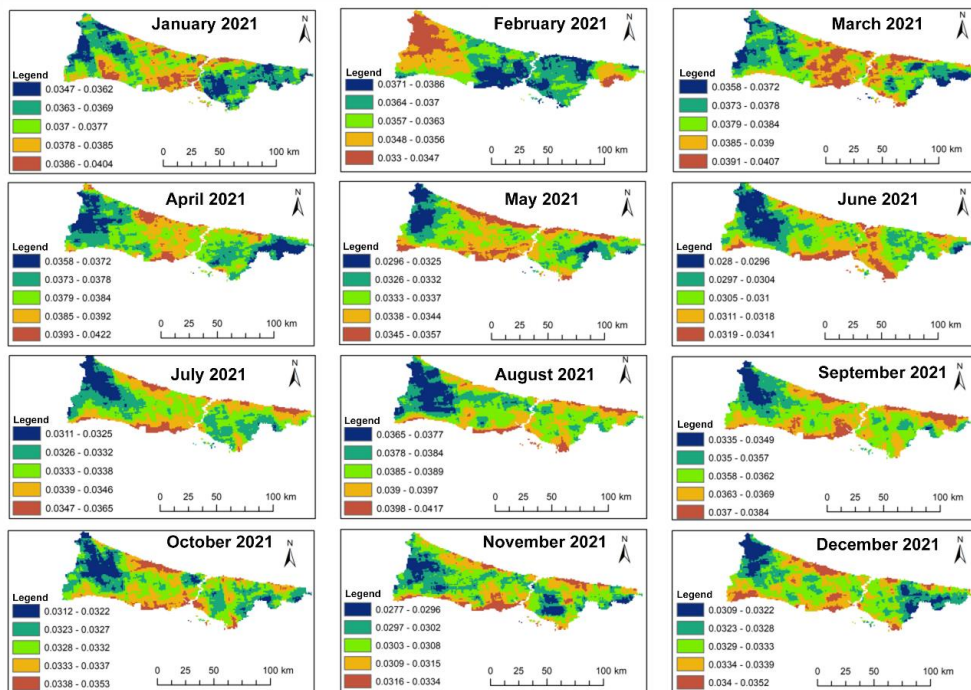


Fig. 15. TROPOMI CO column number density map for 2021.

When the TROPOMI-based Istanbul maps for the O_3 gas are examined, it is observed that the gas has its lowest values mostly in October and November, while its highest value vary between March and April (Figure 16,17,18). According to the previous section, when considering the TROPOMI-based average values, O_3 gas reaches its lowest levels in the autumn months and its highest levels in the spring months. This situation is also similar within the city. O_3 gas has been observed to have a high column number density variation within the city, like SO_2 gas. It has been determined that the areas with high column number density (red) and the areas with low column number density (blue) are intermingled. This has made it

challenging to clearly identify the regions with high and low O_3 gas concentrations in Istanbul.

The annual average column number density values, calculated from the maps obtained from the TROPOMI data are shown in Figure 19.

The correlation between the obtained urban areas and the TROPOMI S5 column number density values were investigated. The analysis revealed a correlation of 0.80 with the CO value, while no significant correlation was found between the other gases. The resulting correlation plots are shown in Figures (20).

The annual average gas concentration values were calculated based on the monthly average gas concentration values obtained for each station for each year. These values are shown in Table 5. The correlation coefficients between the average gas concentration values obtained from ground measurement stations and urbanization were also investigated. A correlation of 0.68

was found with CO, while a strong negative correlation of -0.86 was observed with O₃ (Figure 21).

This study also examined the correlation between ground station data and TROPOMI data. Correlation coefficients of 0.55 and 0.66 were calculated between SO₂ and NO₂ gases, respectively, while low correlations were observed between CO and O₃ gases (Figures 22).

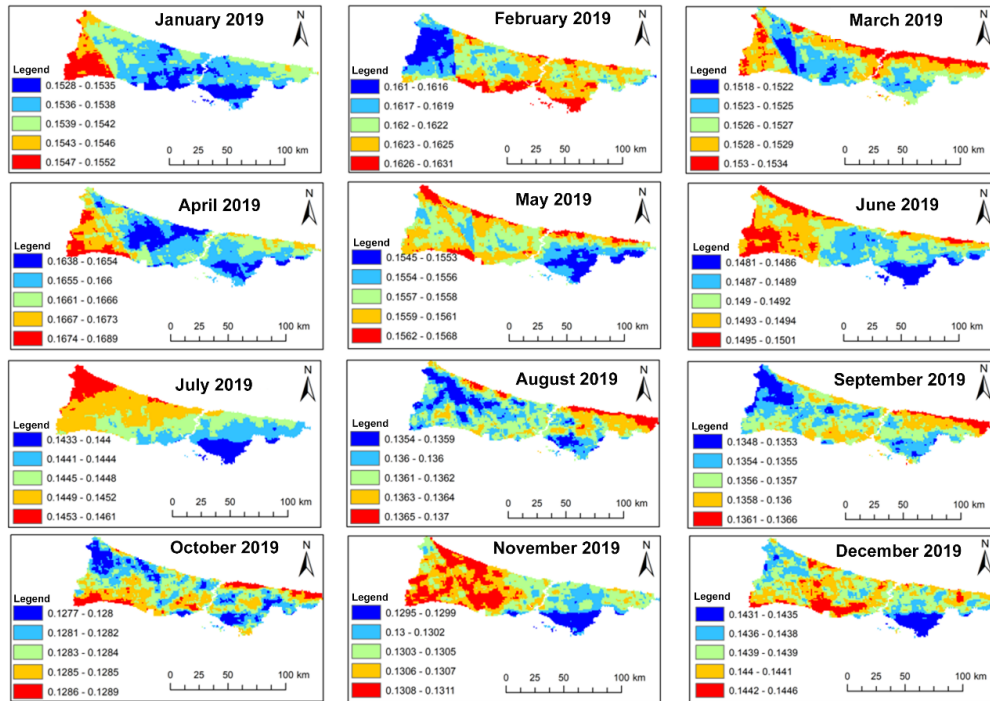


Fig.16. TROPOMI O₃ column number density map for 2019

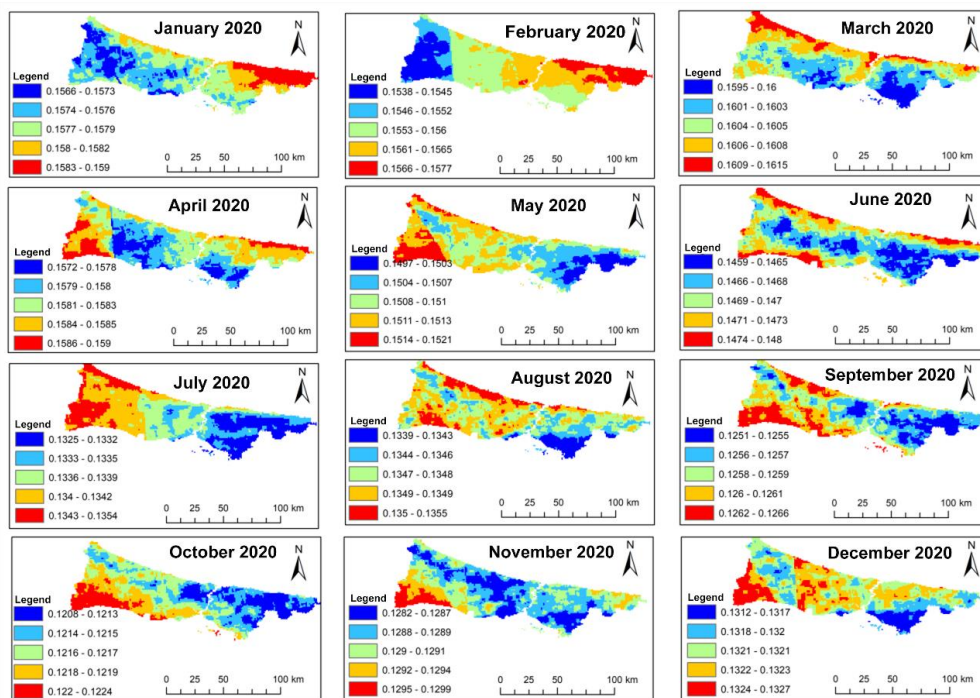


Fig. 17. TROPOMI O₃ column number density map for 2020

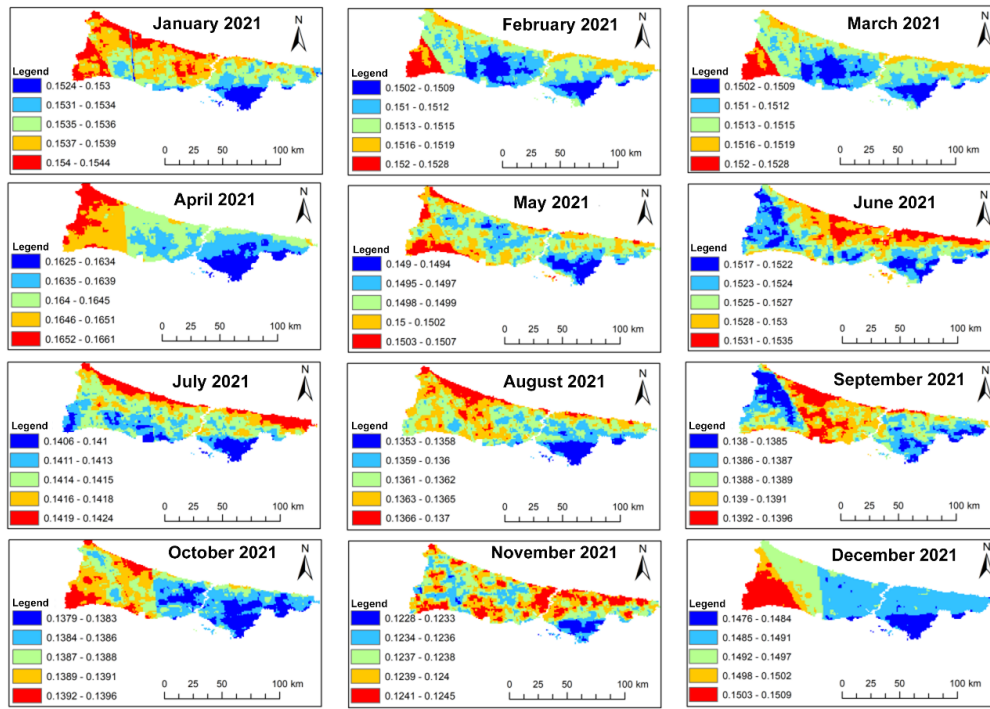


Fig. 18. TROPOMI O₃ column number density map for 2021.

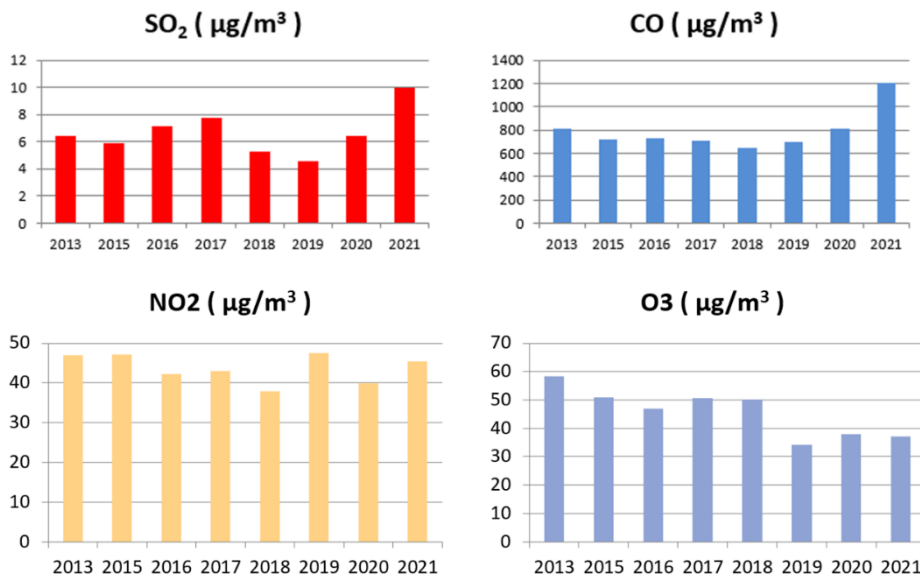


Fig. 19. Gas concentration values of ground measurement stations.

Table 5. Ground measurement station average gas concentration values

Year	SO ₂ (µg/m ³)	CO (µg/m ³)	NO ₂ (µg/m ³)	O ₃ (µg/m ³)
2013	6.367	807.602	46.964	58.210
2015	5.852	715.170	41.446	50.753
2016	7.069	725.048	42.220	47.012
2017	7.678	705.331	43.033	50.702
2018	5.202	645.250	37.866	50.228
2019	4.477	692.887	43.912	36.215
2020	6.378	811.699	39.930	37.882
2021	9.927	1,208.408	45.400	37.090

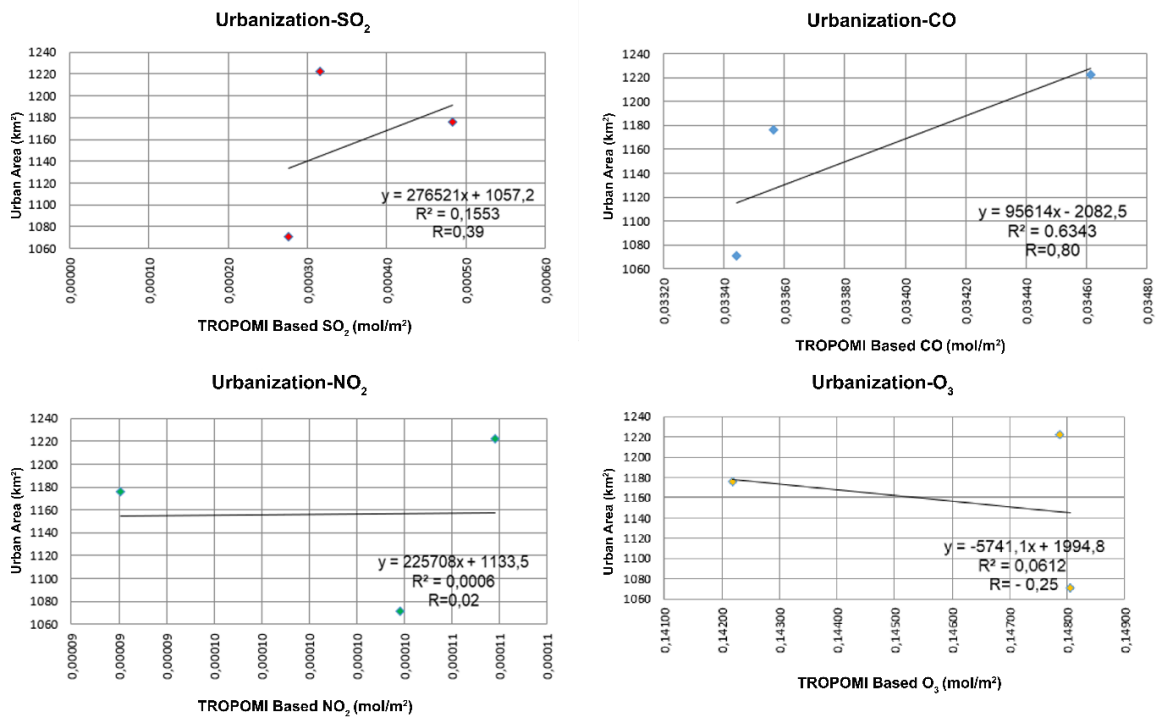


Fig. 20. Urbanization and SO₂ - NO₂ - CO - O₃ correlation analysis based on TROPOMI data

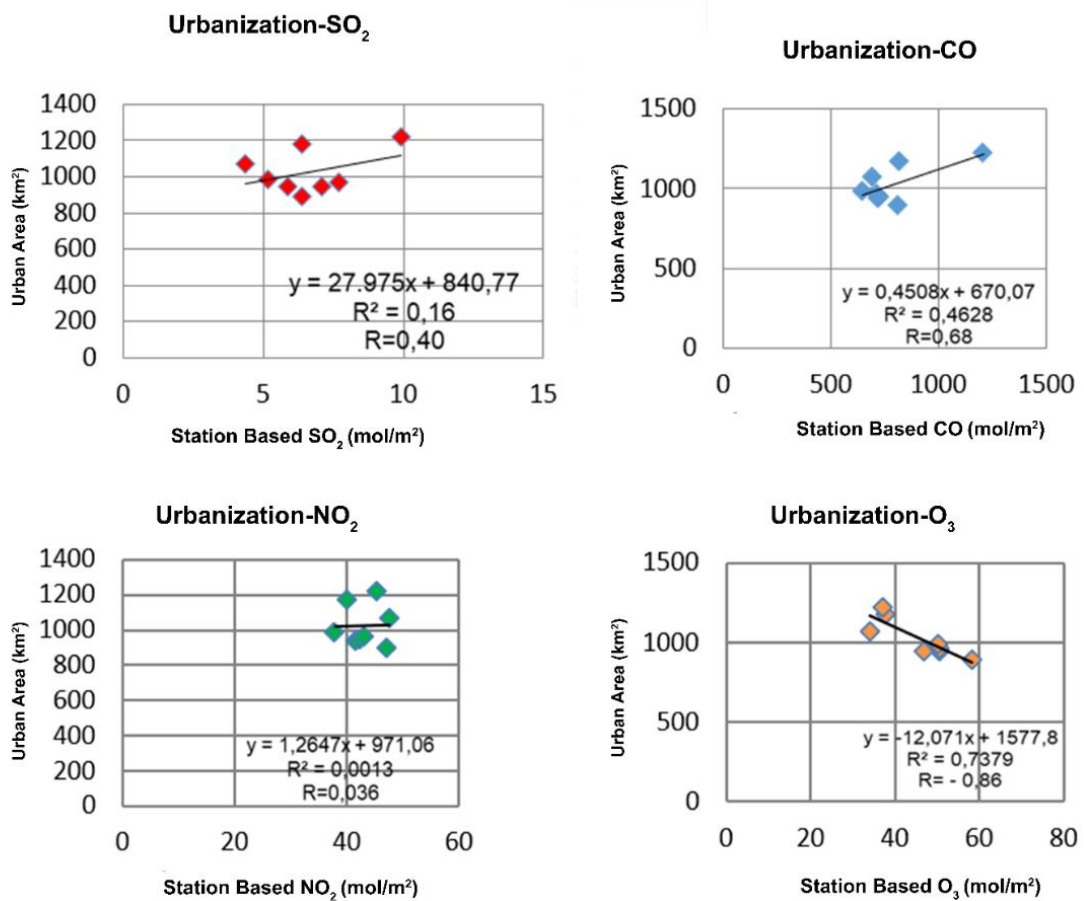


Fig. 21. Urbanization and SO₂ - NO₂ - CO - O₃ correlation analysis based on ground measurement data

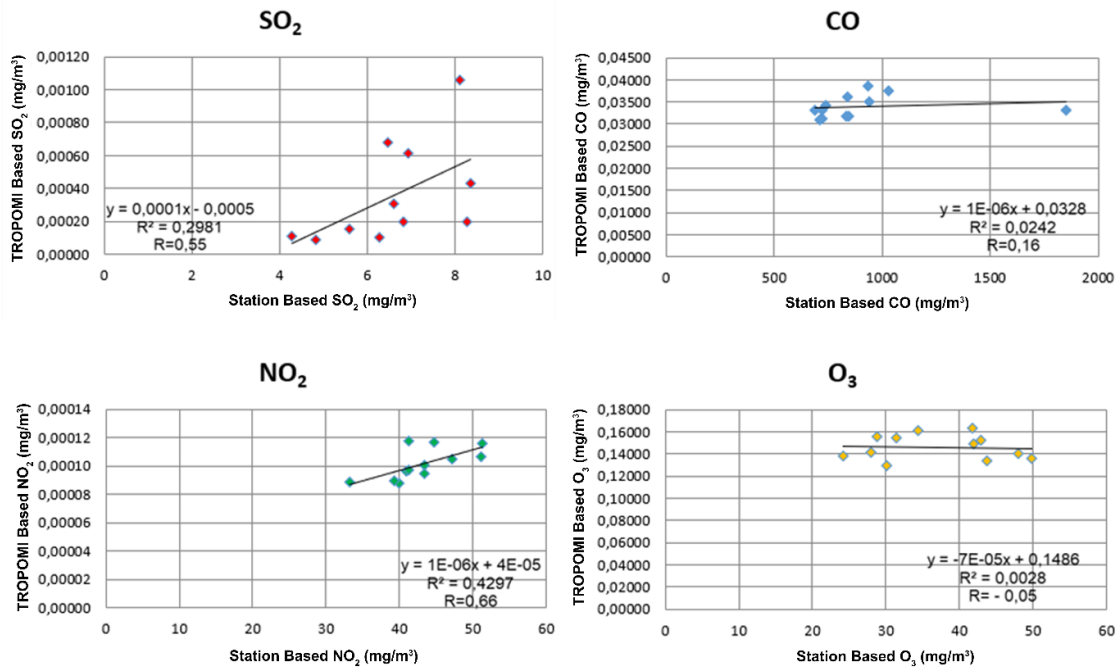


Fig. 28. Correlation analysis between TROPOMI data and ground measuring station for SO₂ - NO₂ – CO - O₃ gas

Discussion and Conclusion

This study investigated the relationship between air pollution and urbanization in Istanbul using data from the Sentinel-5P TROPOMI data and ground stations. The research consisted of three main phases. In the first step, the extent of urbanization was detected using a supervised classification method on the GEE platform. According to the findings, Istanbul's urban land area increased from 499 km² (9% coverage) in 1996 to 1,222 km² (23% coverage) in 2021.

In the second step, gas concentration data based on TROPOMI was obtained, and monthly column number density maps were also created. In the third step, gas data from ground stations were analyzed, revealing monthly, annual, and seasonal variations in the gases. Additionally, the relationship between TROPOMI and ground station data was also investigated.

As a result of the analyses, positive correlations were found between urbanization and TROPOMI column number density values as follows: 0.39 for SO₂, 0.02 for NO₂, 0.80 for CO, and -0.25 for O₃ gases. Additionally, positive correlations were observed between urbanization and ground station-based gas concentration values: 0.40 for SO₂, 0.036 for NO₂, 0.68 for CO, and -0.86 for O₃ gases.

Notably, CO gas exhibited a strong correlation with urbanization in both TROPOMI-based and ground station-based investigations, indicating that an increase in urbanization is associated with an increase in CO gas levels. The correlation between TROPOMI data and ground station values was found to be 0.55 for SO₂, 0.66 for NO₂, 0.16 for CO, and -0.05 for O₃ gases.

This study also observed significant savings time, cost, and labor when using the GEE cloud platform compared to conventional programs. The GEE platform provides

access to a wide range of high-resolution imagery, climate, precipitation, temperature, and other datasets, along with ready-to-use code and algorithms. This is expected to empower decision-makers to conduct rapid analyses on air pollution and its influencing factors.

The findings of this study were determined independently of environmental effects. Future research should explore the relationships between air pollutants and environmental variables such as temperature, wind, humidity, and altitude.

The following recommendations are suggested within the scope of this study:

- Implementation of sustainable policies on renewable energy in conjunction with reducing fossil fuel consumption.
- Increasing the number of air pollution measurement stations nationwide and sharing the data of previously unshared stations with retrospective data.
- Investigating and examining the underlying causes of air pollution in all provinces using scientific methods like RS
- Promoting urban planning adjustments that encourage public transportation and cycling to reduce traffic-related air pollution.
- Conservation and expansion of green spaces.
- Promoting alternative energy sources for residential heating instead of coal.
- Updating legal regulations concerning air pollutants and revising national legal limits affecting public health.

Acknowledgements

This research has not received any specific grant from public, commercial, or non-profit funding agencies. There

are no conflicts of interest among the authors, and it is based on Duygu YASAN's master's thesis.

References

- Achakulwisut, P., Brauer, M., Hystad, P., Anenberg, S. C. (2019). Global, national, and urban burdens of paediatric asthma incidence attributable to ambient NO₂ pollution: estimates from global datasets. *The Lancet Planetary Health*, 3(4), e166–e178. doi.org/10.1016/S2542-5196(19)30046-4
- Aghlmand, M., Kalkan, K., Onur, M. İ., Öztürk, G., Ulutak, E. (2021). Google Earth Engine ile Arazi Kullanımı Haritalarının Üretimi. *Ömer Halisdemir Üniversitesi Mühendislik Bilimleri Dergisi*, 10(1), 38–47. doi.org/10.28948/ngumuh.795977
- Alqurashi, A. F., Kumar, L. (2013). Investigating the Use of Remote Sensing and GIS Techniques to Detect Land Use and Land Cover Change: A Review. *Advances in Remote Sensing*, 02(02), 193–204. doi.org/10.4236/ars.2013.22022
- Arslan, O., Akyürek, Ö. (2018). Spatial Modelling of Air Pollution from PM₁₀ and SO₂ concentrations during Winter Season in Marmara Region (2013-2014). *International Journal of Environment and Geoinformatics*, 5(1), 1-16. doi.org/10.30897/ijgeo.412391
- Burnett, R., Chen, H., Szyszkowicz, M., Fann, N., Hubbell, B., Pope III, C. A., Apte, J. S., Brauer, M., Cohen, A., Weichenthal, S. (2018). Global estimates of mortality associated with long-term exposure to outdoor fine particulate matter. *Proceedings of the National Academy of Sciences*, 115(38), 9592–9597. doi.org/10.1073/pnas.1803222115
- Cakmak, N., Yilmaz, O. S., Sanli, F. B. (2023). Spatio-temporal Analysis of Pollutant Gases using Sentinel-5P TROPOMI Data on the Google Earth Engine during the COVID-19 Pandemic in the Marmara Region , Türkiye. *E-ZBORNIK*, 13(25), 1–14. doi.org/10.47960/2232-9080.2023.25.13.1
- Dong, J., Xiao, X., Menarguez, M. A., Zhang, G., Qin, Y., Thau, D., Biradar, C., Moore, B. (2016). Mapping paddy rice planting area in northeastern Asia with Landsat 8 images, phenology-based algorithm and Google Earth Engine. *Remote Sensing of Environment*, 185, 142–154. doi.org/10.1016/j.rse.2016.02.016
- Engel-Cox, J. A., Hoff, R. M., Haymet, A. D. J. (2004). Recommendations on the use of satellite remote-sensing data for urban air quality. *Journal of the Air and Waste Management Association*, 54(11), 1360–1371. doi.org/10.1080/10473289.2004.10471005
- Engin Duran, H., Pelin Özkan, S. (2015). Trade openness, Urban concentration and city-size growth in Turkey. *Regional Science Inquiry*, 7(1), 35–46.
- Grimm, N. B., Foster, D., Groffman, P., Grove, J. M., Hopkinson, C. S., Nadelhoffer, K. J., Pataki, D. E., Peters, D. P. C. (2008). The changing landscape: Ecosystem responses to urbanization and pollution across climatic and societal gradients. In *Frontiers in Ecology and the Environment* (Vol. 6, Issue 5, pp. 264–272). doi.org/10.1890/070147
- Guo, X., Zhang, Z., Cai, Z., Wang, L., Gu, Z., Xu, Y., Zhao, J. (2022). Analysis of the Spatial–Temporal Distribution Characteristics of NO₂ and Their Influencing Factors in the Yangtze River Delta Based on Sentinel-5P Satellite Data. *Atmosphere*, 13(11). doi.org/10.3390/atmos13111923
- Gupta, P., Christopher, S. A., Wang, J., Gehrig, R., Lee, Y., Kumar, N. (2006). Satellite remote sensing of particulate matter and air quality assessment over global cities. *Atmospheric Environment*, 40(30), 5880–5892. doi.org/10.1016/j.atmosenv.2006.03.016
- He, Y., Wang, C., Chen, F., Jia, H., Liang, D., Yang, A. (2019). Feature Comparison and Optimization for 30-M Winter Wheat Mapping Based on Landsat-8 and Sentinel-2 Data Using Random Forest Algorithm. *Remote Sensing*, 11(5), 535. doi.org/10.3390/rs11050535
- Huang, G., Sun, K. (2020). Non-negligible impacts of clean air regulations on the reduction of tropospheric NO₂ over East China during the COVID-19 pandemic observed by OMI and TROPOMI. *Science of the Total Environment*, 745, 141023. doi.org/10.1016/j.scitotenv.2020.141023
- Kang, Y., Choi, H., Im, J., Park, S., Shin, M., Song, C. K., Kim, S. (2021). Estimation of surface-level NO₂ and O₃ concentrations using TROPOMI data and machine learning over East Asia. *Environmental Pollution*, 288(2), 117711. doi.org/10.1016/j.envpol.2021.117711
- Kaplan, G., Yigit Avdan, Z. (2020). Space-Borne Air Pollution Observation From Sentinel-5P Tropomi: Relationship Between Pollutants, Geographical and Demographic Data. *International Journal of Engineering and Geosciences*, 2, 130–137. doi.org/10.26833/ijeg.644089
- Kumar, L., Mutanga, O. (2018). Google Earth Engine applications since inception: Usage, trends, and potential. *Remote Sensing*, 10(10), 1–15. doi.org/10.3390/rs10101509
- Kural, G., Balkıs, N. Ç., Aksu, A. (2018). Source identification of Polycyclic Aromatic Hydrocarbons (PAHs) in the urban environment of İstanbul. *International Journal of Environment and Geoinformatics*, 5(1), 53–67.
- Lelieveld, J., Pozzer, A., Pöschl, U., Fnais, M., Haines, A., Münzel, T. (2020). Loss of life expectancy from air pollution compared to other risk factors: A worldwide perspective. *Cardiovascular Research*, 116(11), 1910–1917. doi.org/10.1093/cvr/cvaa025
- Liu, D., Chen, N., Zhang, X., Wang, C., Du, W. (2020). Annual large-scale urban land mapping based on Landsat time series in Google Earth Engine and OpenStreetMap data: A case study in the middle Yangtze River basin. *ISPRS Journal of Photogrammetry and Remote Sensing*, 159, 337–351.
- Liu, X., Hu, G., Chen, Y., Li, X., Xu, X., Li, S., Pei, F., Wang, S. (2018). High-resolution multi-temporal mapping of global urban land using Landsat images based on the Google Earth Engine Platform. *Remote Sensing of Environment*, 209(February), 227–239. doi.org/10.1016/j.rse.2018.02.055
- Magro, C., Nunes, L., Gonçalves, O., Neng, N., Nogueira, J., Rego, F., Vieira, P. (2021). Atmospheric Trends of CO and CH₄ from Extreme Wildfires in Portugal

- Using Sentinel-5P TROPOMI Level-2 Data. *Fire*, 4(2), 25. doi.org/10.3390/fire4020025
- Martin, R. V. (2008). Satellite remote sensing of surface air quality. *Atmospheric Environment*, 42(34), 7823–7843.
- Patel, N. N., Angiuli, E., Gamba, P., Gaughan, A., Lisini, G., Stevens, F. R., Tatem, A. J., Trianni, G. (2015). Multitemporal settlement and population mapping from landsat using google earth engine. *International Journal of Applied Earth Observation and Geoinformation*, 35(PB), 199–208. doi.org/10.1016/j.jag.2014.09.005
- Potts, D. A., Marais, E. A., Boesch, H., Pope, R. J., Lee, J., Drysdale, W., Chipperfield, M. P., Kerridge, B., Siddans, R., Moore, D. P., Remedios, J. (2021). Diagnosing air quality changes in the UK during the COVID-19 lockdown using TROPOMI and GEOS-Chem. *Environmental Research Letters*, 16(5). doi.org/10.1088/1748-9326/abde5d
- Raja, R. A. A., Anand, V., Kumar, A. S., Maithani, S., Kumar, V. A. (2013). Wavelet Based Post Classification Change Detection Technique for Urban Growth Monitoring. *Journal of the Indian Society of Remote Sensing*, 41(1), 35–43. doi.org/10.1007/s12524-011-0199-7
- Saadat, H., Adamowski, J., Bonnell, R., Sharifi, F., Namdar, M., Ale-Ebrahim, S. (2011). Land use and land cover classification over a large area in Iran based on single date analysis of satellite imagery. *ISPRS Journal of Photogrammetry and Remote Sensing*, 66(5), 608–619. doi.org/10.1016/j.isprsjprs.2011.04.001
- Sünsüli, M., Kalkan, K. (2022). Sentinel-5P uydu görüntüleri ile azot dioksit (NO₂) kirliliğinin izlenmesi. *Türkiye Uzaktan Algılama Dergisi*, 4(1), 1–6.
- Tømmervik, H., Johansen, B. E., Pedersen, J. P. (1995). Monitoring the effects of air pollution on terrestrial ecosystems in Varanger (Norway) and Nikel-Pechenga (Russia) using remote sensing. *Science of the Total Environment*, 160, 753–767.
- Tyagi, S., Garg, N., Paudel, R. (2014). Environmental Degradation: Causes and Consequences. *European Researcher*, 81(8–2), 1491. doi.org/10.13187/er.2014.81.1491
- Vos, K., Splinter, K. D., Harley, M. D., Simmons, J. A., Turner, I. L. (2019). CoastSat: A Google Earth Engine-enabled Python toolkit to extract shorelines from publicly available satellite imagery. *Environmental Modelling and Software*, 122(June), 104528. doi.org/10.1016/j.envsoft.2019.104528
- Wang, S., Hao, J. (2012). Air quality management in China: Issues, challenges, and options. *Journal of Environmental Sciences*, 24(1), 2–13. doi.org/10.1016/S1001-0742(11)60724-9
- Wong, B. A., Thomas, C., Halpin, P. (2019). Automating offshore infrastructure extractions using synthetic aperture radar & Google Earth Engine. *Remote Sensing of Environment*, 233(November 2018), 111412. doi.org/10.1016/j.rse.2019.111412
- Yılmaz, O. S., Acar, U., Sanli, F. B., Gulgen, F., Ates, A. M. (2023). Mapping burn severity and monitoring CO content in Türkiye’s 2021 Wildfires, using Sentinel-2 and Sentinel-5P satellite data on the GEE platform. *Earth Science Informatics*, 16(1), 221–240. doi.org/10.1007/s12145-023-00933-9
- Yuan, F., Sawaya, K. E., Loeffelholz, B. C., Bauer, M. E. (2005). Land cover classification and change analysis of the Twin Cities (Minnesota) metropolitan area by multitemporal Landsat remote sensing. *Remote Sensing of Environment*, 98(2–3), 317–328. doi.org/10.1016/j.rse.2005.08.006
- URL-1. <https://data.tuik.gov.tr> (25.04.2022)
- URL-2 <https://www.tripreport.com/cities/> (25.04.2022)
- URL-3 <https://web.archive.org> (25.04.2022)
- Ülker, D., Bayırhan, İ., Mersin, K., Gazioğlu, C. (2021). A comparative CO₂ emissions analysis and mitigation strategies of short-sea shipping and road transport in the Marmara Region. *Carbon Management*, 12(1), 1–12.